Bioelectrochemistry 165 (2025) 108971

Contents lists available at ScienceDirect

Bioelectrochemistry

journal homepage: www.journals.elsevier.com/bioelectrochemistry

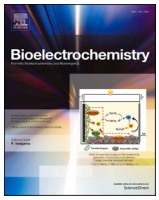

Study on effect of electroporation combining high- and low-frequency harmonics

Borja López-Alonso [a,*], Tamara Polajžer [b], Matej Reberšek [b], Héctor Sarnago [a], Óscar Lucía [a], Damijan Miklavčič [b]

[a] Electronic Engineering and Communications Department, I3A, Universidad de Zaragoza. Maria de Luna, 1, 50018 Zaragoza. Spain.
[b] Faculty of Electrical Engineering. University of Ljubljana, Tržaška 25, 1000, Ljubljana. Slovenia

ARTICLE INFO

Keywords:
Electroporation
Radiofrequency
Power electronics

ABSTRACT

The effects of electroporation are highly influenced by the shape of the applied waveform. This waveform shape can modify the transmitted energy and current flow patterns, impacting the electric field distribution, temperature rise among others. These interactions, along with their synergies with electroporation, are being explored across various industrial and research domains. For instance, in the biomedical field, high-frequency waveforms such as nanosecond pulses offer distinct advantages, while in the food industry, controlled temperature increases combined with electroporation are beneficial. However, in the medical field, the effects of combining high-frequency waveforms (in the MHz range) with low-frequency waveforms (in the kHz range commonly used in clinical electroporation) have not been thoroughly studied, though hypotheses have been proposed regarding their potential effects.

In this paper, proof of concept of the effect of the combination of two harmonics is presented using three different strategies to investigate new electroporation protocols. To support this study, a specialized electrical and thermal test bench was developed to control and evaluate the feasibility and potential of possible synergy between high- and low-frequency waveforms to electroporation using an *in vitro* model.

1. Introduction

Electroporation is a phenomenon characterized by the increased permeability of cell membrane caused by induction of a transmembrane electrical potential [1]. Increased permeability, whether transient or permanent, results from biophysical and biochemical changes in the membrane that are still being actively studied [2]. Electroporation depends on several factors, the most significant of which are the amplitude and shape of the applied electric field, such as its intensity, duration, and frequency [3,4]. This electric field is generated by means of the application of an electric waveform whose characteristics together with the application system define the properties of the electric field. Nowadays, the most common waveform in electroporation applications are exponential decay, monopolar or monophasic, or bipolar or biphasic square pulses [5], which are characterized by its peak voltage V_P, duration t_{ON}, rise t_r, fall time t_f, and polarity (Fig. 1). The above waveform has demonstrated its effectiveness, but in order to control the effects of electroporation it is necessary to better understand the used waveforms and explore new approaches and their specific advantages or/and disadvantages [3,6,7].

In the field of voltage waveforms applied to electroporation, the most studied parameters are amplitude, shape, and frequency [3], all of which have been shown to strongly affect the outcomes of electroporation. Early electroporation protocols, limited in part by technological constraints, established clinical standards based on pulses with a duration of few tens of μs [8], and thus relied on waveforms in the kHz range. Although these waveforms have proven to be effective, alternative approaches such as high-frequency irreversible electroporation (H-FIRE) [7] or electroporation with nanosecond pulses [9,10] have emerged over time due to advances in electronic technology. New hardware developments enabled exploration of various benefits associated with higher frequencies, such as reduced muscle contractions [11–13], improved treatment homogeneity [5,14–16], and enhanced intracellular effects [17]. However, these advantages come at a cost: due to the frequency dependence of electroporation, increasing the amplitude is required to compensate for higher frequencies. Additionally, the

* Corresponding author.
E-mail address: blopez@unizar.es (B. López-Alonso).

https://doi.org/10.1016/j.bioelechem.2025.108971
Received 26 December 2024; Received in revised form 19 February 2025; Accepted 10 March 2025
Available online 17 March 2025

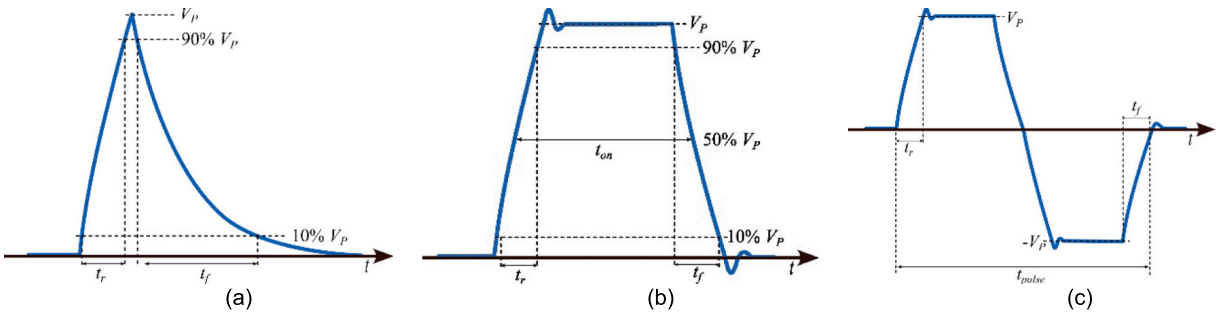

Fig. 1. Realistic waveforms in electroporation applications [5]: (a) Exponential decay pulse, (b) monopolar or monophasic pulse, and (c) bipolar or biphasic pulse.

inherently capacitive nature of biological tissues causes the applied currents to rise with frequency, reducing the energy efficiency of treatments.

Given the benefits associated with different frequency ranges, combining them could generate intermediate effects or potential synergies, leading to treatments that are more efficient than those at high frequencies while preserving their advantages. This approach could provide novel and valuable insights into electroporation applications.

To carry out a proof of concept test for this idea, the simplest method is to directly combine two sinusoidal functions or fundamental harmonics of different frequencies. By adjusting the frequency and amplitude of these sinusoidal waves, new strategies can be explored to improve the control and effectiveness of electroporation. This combination can be implemented in various complex ways, but the three most basic methods are addition, multiplication, and sequential application. In this work, these three approaches have been investigated through three strategies that may be of interest for electroporation applications: harmonic addition, amplitude modulation, and sequential application.

Given the potentially valuable effects of these three strategies combining high- and low-frequency harmonics in electroporation, this study presents a proof of concept test using an *in vitro* model to assess their feasibility and to evaluate initial hypotheses regarding their effects. This study required a specialized electronic and thermal setup to test each strategy, enabling us to analyze both immediate and long-term effects of these waveforms across various protocols and *in vitro* cell testing to study the potential synergy as well as provide proof of concept.

2. Methods

2.1. In vitro model

To conduct this proof of concept, an *in vitro* model was selected for its ability to simplify electronic design requirements and enable straightforward, cost-effective experimentation. Additionally, two widely used cell lines in electroporation research were chosen to support robust conclusions. The first, Chinese hamster ovary (CHO) cells, commonly used in electroporation studies [18–20]. Second, heart myoblast (H9c2) cells are commonly used as a model for heart tissue [21–23]. With both cell lines, aluminum electroporation cuvettes with 1 mm distance were used for the application of the different waveforms. Both cell lines were purchased from the European Collection of Authenticated Cell Cultures. CHO cells were grown in HAM F-12 growth medium (PAA, Austria) and H9c2 in Dulbecco's Modified Eagle's Medium (DMEM) growth medium (Sigma-Aldrich, USA). Both media were supplemented with 10 % fetal bovine serum (FBS, Sigma-Aldrich, USA), L-glutamine (0.5 % for CHO, 2 % for H9c2) (StemCell, Canada), penicillin/streptomycin (PAA, Austria) and 0.1 % gentamycin (Sigma- Aldrich, USA). Cells were grown in an incubator at 37 °C with controlled atmosphere (CHO at 5 % CO_2, H9c2 at 10 % CO_2) until 70–80 % confluency was reached. For experiment growth medium was removed and the trypsin-EDTA (PAA, Austria) was used to detach cells. Afterwards fresh medium was added to inactivate trypsin. Cell suspension was centrifuged at 180*g* for 5 min, supernatant was removed, and cells were resuspended in fresh growth media (CHO in HAM, H9c2 in DMEM) to obtain a concentration of 1×10^6 cells/ml.

2.2. Versatile waveform generator for combining different harmonics

To evaluate the three proposed strategies, it was necessary to synthesize a high-frequency, high-amplitude waveforms that enable the combination of high- and low-frequency harmonics in wide range of proportions. As no commercial generators met those performance requirements in electroporation, a custom design was needed.

The power electronics generator used in this research has been designed *ad-hoc* and implemented by the Group of Power Electronics and Microelectronics (GEPM) of the University of Zaragoza. It is based on a multilevel topology that enables versatile operation and waveform generation [24]. As it is shown in Scheme 1, the converter consists of an isolated rectifier directly connected to the AC mains (vac), which supplies an inverter with the voltage $V_{r,LF}$. The inverter feeds *n* independent transformers, which, together with a controlled rectifier, form an isolated DC-DC converter that generates the voltage $v_{dc,n}$. This voltage is used by the inverters at each level that generates voltages $v_{o,i}$. These inverters are connected in series at the output to generate the final output voltage, v_o, which is the summation of *n* individual output voltages, $v_{o,i}$.

Through digital control implemented *via* an FPGA, commanded by fiber optics and running a custom application on a PC, the complete structure functions as a high-voltage versatile waveform generator. This system enables the synthesis of arbitrary waveforms with a bandwidth up to 2 MHz, a peak-to-peak voltage above 600 V, and a maximum output current of 15 A peak.

The proposed system was designed to allow flexible application for any voltage waveform in electroporation cuvettes.

The prototype was monitored throughout all procedures using a WaveSurfer 3054(Teledyne LeCroy, Chestnut Ridge, NY, USA) oscilloscope, equipped with an HVD3102A (Teledyne LeCroy, Chestnut Ridge, NY, USA) differential voltage probe and a CP030 (Teledyne LeCroy, Chestnut Ridge, NY, USA) current probe. Finally, voltage measurements were made directly on the custom-made cuvette holder, ensuring accurate measurement.

2.3. Temperature monitoring

To fully characterize the experimental setup and monitor temperature variations, accurate real-time temperature measurements were required for samples subjected to high-voltage pulses. A fiber optic sensor system (opSens, Québec, QC, Canada) was employed, consisting of a ProSens signal conditioner and an OTG-F fiber optic temperature sensor, providing a resolution of 0.1 °C and a sampling rate of one measurement every 0.1 s. To ensure precise and repeatable sensor placement, a custom-designed 3D-printed micromanipulator was developed (Fig. 2 (a)).

The micromanipulator allowed three-dimensional positioning of the probe within the cuvette, ensuring it remained in the center of the

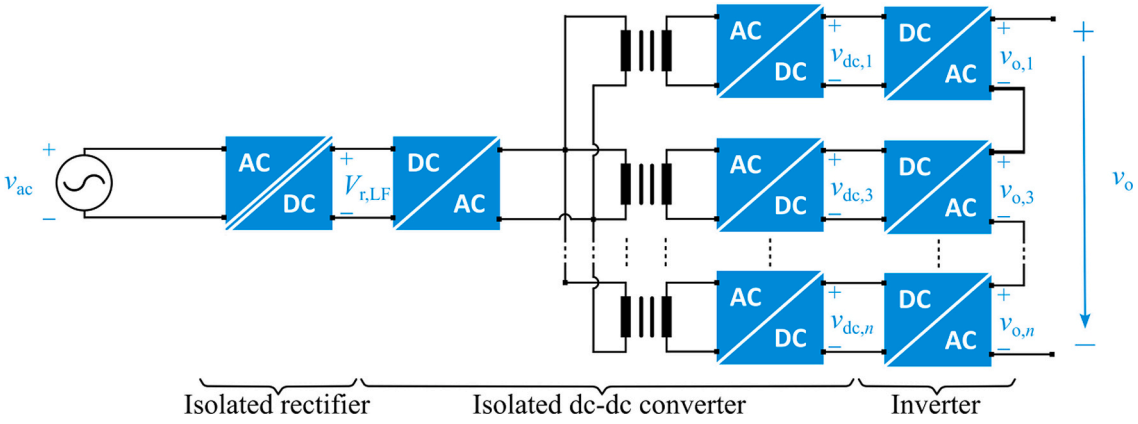

Scheme. 1. Block diagram of the proposed multi-level converter for versatile waveform generation.

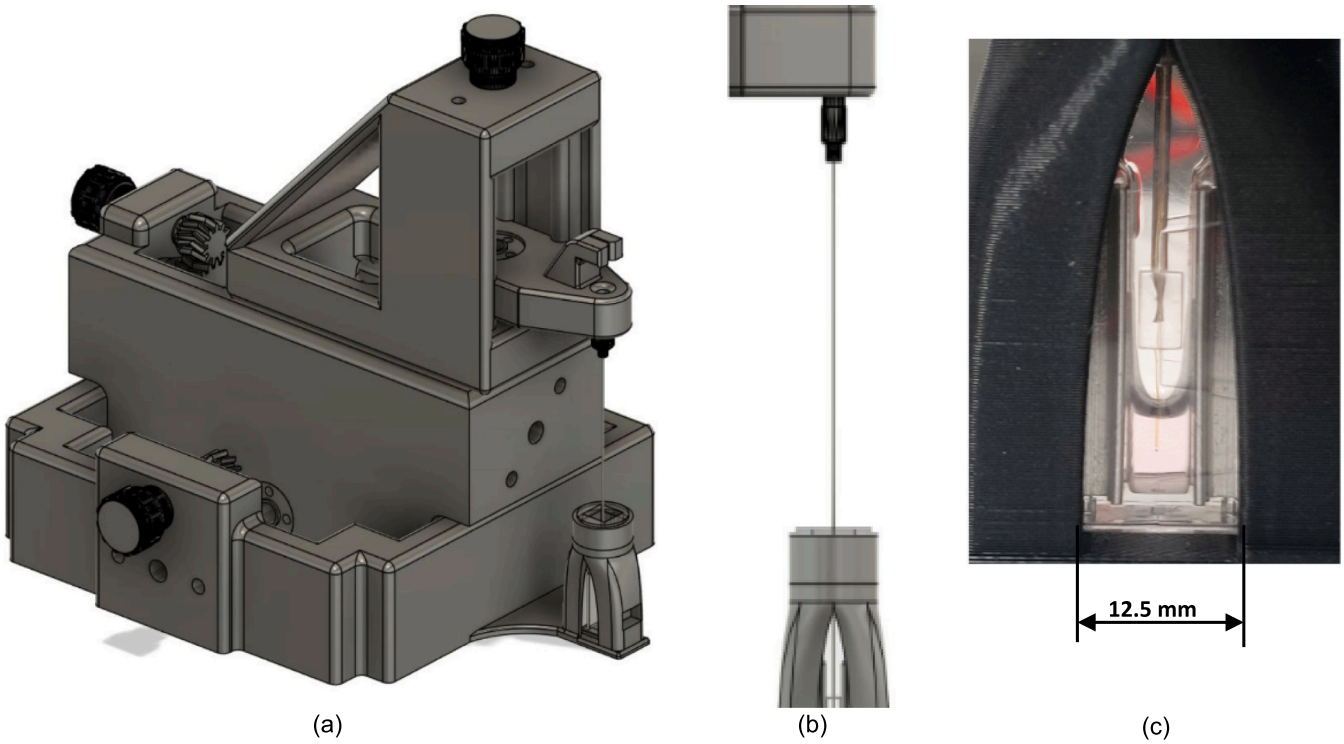

Fig. 2. Temperature measurement system: (a) Scheme of 3D-printed device with cuvette holder and temperature probe, (b) Scheme of 3D-printed cuvette holder and temperature probe, and (c) real example of probe placement.

sample without contacting the electrodes or the cuvette walls (Fig. 2 (b) and Fig. 2 (c)). It was fabricated using 3D printing technology, employing a Creality Ender 3 V2 and Prusa MK4 with PLA filament for durability and ease of use. The design was created in Autodesk Fusion 360 and processed with Ultimaker Cura for slicing and G-code generation. To ensure structural stability and precise adjustments, M4 brass inserts were embedded for threaded connections, and trapezoidal lead screws (2 mm pitch) enabled fine linear control. Given the ±0.25 mm printing tolerance, post-processing adjustments were made, including the application of adhesive tape to guiding structures to improve stability. This integrated measurement system successfully enabled real-time thermal monitoring with high spatial accuracy, ensuring reliable temperature measurements during electroporation experiments.

2.4. Different waveforms and treatment protocols

The proposed proof of concept aimed to evaluate three different strategies, each requiring a different modulation protocol. However, to achieve complementary and comparable results, all strategies were based on applying voltage bursts with a duration of 5 ms to electroporation cuvettes of 1 mm gap containing 60 µl cell suspension. The applied voltages have been adjusted in each experiment, considering the features of the generator and the response of each cell line used. The low-frequency values correspond to those reported in the literature for traditional electroporation applications [3,4], while the high-frequency values fall within the radiofrequency range and are constrained by the limitations of the proposed generator.

To compare the effects of the different protocols, specifically the various applied voltage waveforms $v(t)$, their peak amplitude V_P and root mean square value V_{RMS} were used. Although comparing an electroporation protocol typically requires only the V_P which is proportional to the maximum applied electric field, the wide variation in waveform shapes used also makes it necessary to consider the V_{RMS}, which is proportional to the energy delivered, and is calculated based on the

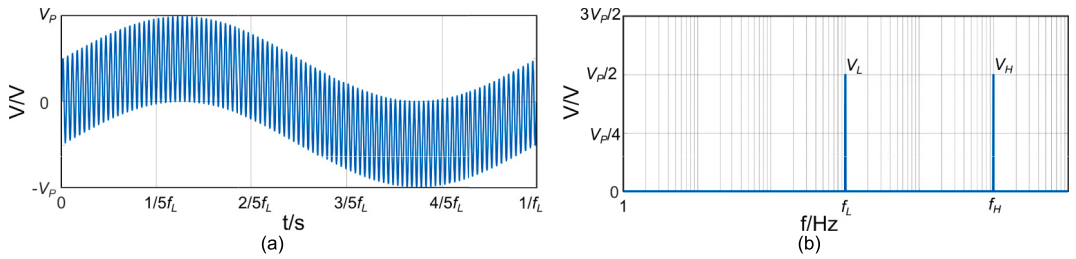

Fig. 3. Harmonic addition waveform: (a) temporal waveform, and (b) harmonic content.

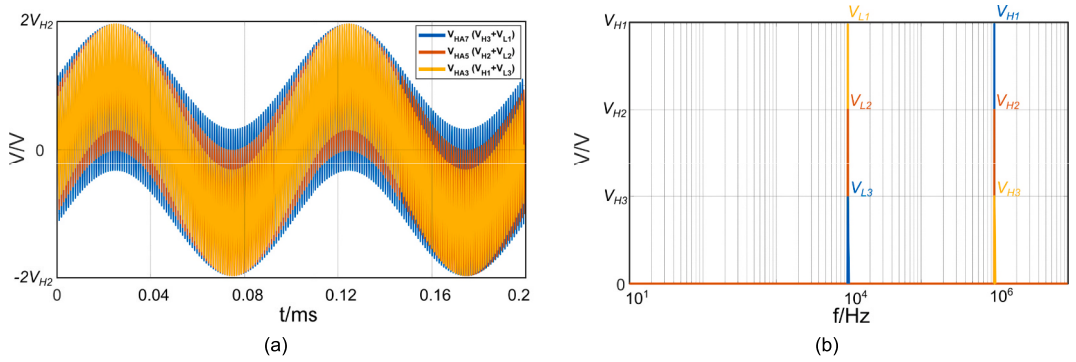

Fig. 4. Three representative protocols of harmonic addition: (a) temporal waveform, and (b) harmonic content.

waveform's period T:

$$V_{RMS} = \sqrt{\frac{1}{T}\int_{T} v(t)^2 dt} \quad (1)$$

With all the above considerations, the protocols for evaluating the three strategies: harmonic addition, amplitude modulation and sequential application.

Harmonic addition is a strategy involving a combination of two harmonics with very different frequencies through direct addition. Direct combination of the two waveforms allows for the exploration of potential synergies between their different properties, enhancing beneficial effects. This approach may be particularly valuable for developing protocols that minimize electrochemical reactions, enhance efficiency, or increase molecular mobility due to the enhanced energy transfer and the high-frequency electromagnetic field variations produced with high-frequency waves.

Harmonic addition waveform $v_{HA}(t)$, as shown in Fig. 3 (a), consisted of the sum of two sine functions with amplitudes of V_H and V_L, and frequencies of f_L and f_H, respectively:

$$v_{HA}(t) = V_L sin(2\pi f_L t) + V_H sin(2\pi f_H t) \quad (2)$$

Its Fast Fourier Transform (Fig. 3 (b)) shows two harmonics well separated in frequency. In this case, it was essential to examine the influence of each harmonic within the combined waveform and to compare these results with those of the individual harmonics.

To achieve the desired comparison, the same burst durations and number of bursts were used, studying three purely sinusoidal high-frequency protocols V_{H1_3} and three low-frequency V_{L1_3} ones. These treatments were then combined into nine different protocols V_{HA1_9} with all results compared in terms of V_{RMS}, V_P, and the amplitude of the two harmonics, high-frequency V_H and low-frequency V_L that compose the waveform. In this experiment, the amplitudes of the pure sine waves, V_H and V_L, were adjusted for each cell line to enhance the sensitivity of the tests. Since the behavior of each cell line differs, the temporal parameters were fixed, and the maximum amplitudes of the treatments were modified based on the behavior of the cell line models. This adjustment ensured that the observed response in both cell lines covered the full sensitivity range of the test, from 0 to 100 %.

Fig. 4 illustrates three representative protocols used to evaluate the

Table 1
Purely Sinusoidal Protocols in CHO.

	V_P (V)	V_{RMS} (V)	f (kHz)	Duration (ms)	N Burst
V_{H1}	85	60.1	1000	5	20
V_{H2}	76.5	54.1	1000	5	20
V_{H3}	61	43.1	1000	5	20
V_{L1}	85	60.1	10	5	20
V_{L2_1}	81	57.3	10	5	20
V_{L2_2}	70	49.5	10	5	20
V_{L3}	61	43.1	10	5	20

Table 2
Harmonic Addition Protocols in CHO.

	Combination	V_{RMS} (V)	Duration (ms)	N Burst
V_{HA1}	$V_{H1} + V_{L1}$	85	5	20
V_{HA2}	$V_{H1} + V_{L2\_1}$	83	5	20
V_{HA3}	$V_{H1} + V_{L2\_2}$	77.9	5	20
V_{HA4}	$V_{H1} + V_{L3}$	74	5	20
V_{HA5}	$V_{H2} + V_{L1}$	80.9	5	20
V_{HA6}	$V_{H2} + V_{L2\_2}$	78.8	5	20
V_{HA7}	$V_{H2} + V_{L2\_2}$	73.3	5	20
V_{HA8}	$V_{H2} + V_{L3}$	69.2	5	20
V_{HA9}	$V_{H3} + V_{L1}$	74	5	20
V_{HA10}	$V_{H3} + V_{L2\_1}$	71.7	5	20
V_{HA11}	$V_{H3} + V_{L2\_2}$	65.6	5	20
V_{HA12}	$V_{H3} + V_{L3}$	61	5	20

Table 3
Purely Sinusoidal Protocols in H9c2.

	V_P (V)	V_{RMS} (V)	f (kHz)	Duration (ms)	N Burst
V_{H1}	80	56.6	10	5	20
V_{H2}	67.5	47.7	10	5	20
V_{H3}	55	38.9	10	5	20
V_{L1}	80	56.6	1000	5	20
V_{L2}	67.5	47.7	1000	5	20
V_{L3}	55	38.9	1000	5	20

Table 4
Harmonic Addition Protocols in H9c2.

	Combination	V_{RMS} (V)	Duration (ms)	N Burst
V_{HA1}	$V_{H1} + V_{L1}$	80	5	20
V_{HA2}	$V_{H1} + V_{L2}$	74	5	20
V_{HA3}	$V_{H1} + V_{L3}$	68.7	5	20
V_{HA4}	$V_{H2} + V_{L1}$	74	5	20
V_{HA5}	$V_{H2} + V_{L2}$	67.5	5	20
V_{HA6}	$V_{H2} + V_{L3}$	61.6	5	20
V_{HA7}	$V_{H3} + V_{L1}$	68.7	5	20
V_{HA8}	$V_{H3} + V_{L2}$	61.6	5	20
V_{HA9}	$V_{H3} + V_{L3}$	55	5	20

harmonic addition strategy. Fig. 4 (a) shows the temporal waveforms and Fig. 4 (b) details their harmonic content.

For the CHO cell line, the protocols used are detailed in Table 1 and Table 2 Following the initial analyses, it was determined that four additional experiments would be necessary to explore the effect of the low-frequency harmonic in greater detail. To achieve this, the V_{L2} protocol was divided into V_{L2_1} and V_{L2_2}, allowing for more precise evaluation of the harmonic's influence. Consequently, 12 harmonic addition protocols were analyzed, instead of the 9 initially proposed.

The protocols for the H9c2 line are presented in Table 3 and Table 4 remaining unchanged from their initial conceptualization.

The second strategy is amplitude modulation, in which two high-frequency harmonics of equal amplitude, in the MHz range, are used to synthesize a waveform with an envelope frequency in the kHz range. However, unlike direct addition, this method produces a wave with purely high-frequency harmonic content. Meaning that, to achieve low-frequency waveform effects, the cell membrane must present non-linear behavior. Although the role of the membrane as a signal filter, due to its intrinsic capacitive properties, is well documented [25], its non-linear behavior is less understood. Moreover, if cells exhibit non-linear behavior at the membrane level, and considering that many undesirable low-frequency effects, such as electrolysis, occur primarily extracellularly, this approach could enable more selective electroporation.

Amplitude modulation waveform $v_{AM}(t)$, as shown in Fig. 5 (a), consisted of the multiplication of two sine functions with an amplitude V_P, and frequencies of f_c and f_e, respectively:

$$v_{AM}(t) = V_P sin(2\pi f_c t) \cdot sin(2\pi f_e t) \quad (3)$$

This waveform is characterized by a high-frequency oscillation f_c enveloped by low-frequency f_e modulation. To achieve a constant envelope shape, as shown in Fig. 5 (b), this waveform was formed from two harmonics of equal amplitude, with the envelope frequency determined by small frequency difference between these harmonics.

The objective of this approach was to evaluate whether the shape of the envelope enhances the efficiency of the wave for electroporation compared to a pure high-frequency wave, and to investigate if the frequency of this envelope affects the results. To do this, the same burst durations and number of bursts were used, studying 4 purely sinusoidal high-frequency treatments with two different carrier frequencies f_c. For each of these two carrier frequencies, f_c, two different amplitudes were evaluated. First, the peak value of the amplitude-modulated waveform

Table 5
Purely Sinusoidal Protocols in CHO and H9c2.

	V_P (V)	V_{RMS} (V)	f_c (kHz)	f_e (kHz)	Duration (ms)	N Burst
V_{1M_P}	200	141	1000	0	5	20
V_{1M_RMS}	141	100	1000	0	5	20
V_{500K_P}	150	106	500	0	5	20
V_{500K_RMS}	106	75	500	0	5	20

Table 6
Amplitude Modulation Protocols in CHO and H9c2.

	V_P (V)	V_{RMS} (V)	f_c (kHz)	f_e (kHz)	Duration (ms)	N Burst
V_{AM1}	200	100	1000	1	5	20
V_{AM2}	200	100	1000	10	5	20
V_{AM3}	200	100	1000	50	5	20
V_{AM4}	200	100	1000	100	5	20
V_{AM5}	150	75	500	1	5	20
V_{AM6}	150	75	500	10	5	20
V_{AM7}	150	75	500	50	5	20
V_{AM8}	150	75	500	100	5	20

V_P was evaluated whether changes in the waveforms shape improved performance at the same peak level. Then, the amplitude that achieved the same V_{RMS} as the modulated waveform was determined, allowing to compare the performance of both waveform shapes under equivalent transmitted energy conditions. The parameters from these purely sinusoidal treatments were used to set the V_P of 8 different amplitude-modulated treatments, 4 for each f_c, in which f_e was modified.

The protocols for the CHO and H9c2 line are presented in Table 5 and Table 6, remaining unchanged from their initial conceptualization.In this experiment, 20 bursts of 5 ms were used with two f_c selected: 1 MHz and 500 kHz (Table 5). For each f_c, 4 amplitude-modulated protocols V_{AM} were applied with f_e ranging from 1 kHz to 100 kHz, resulting in 8 different amplitude-modulated treatments (Table 6).

Fig. 6 shows shows two representative protocols used to evaluate amplitude modulation strategy. Fig. 6 (a) shows the temporal waveforms and Fig. 6 (b) details their harmonic content. For CHO and H9c2 cell lines, the protocols used to evaluate amplitude modulation strategy are detailed in Table 5 and Table 6.

The third strategy is a sequential application, which involves the consecutive application of two harmonics. Unlike the previous approaches, this method does not aim to combine high- and low-frequency electroporation effects or to localize treatment effects. Instead, it seeks to enhance electroporation outcomes through sample temperature modulation. Similar to clinical applications of radiofrequency [26], a waveform in the MHz range can be applied to achieve ohmic heating, allowing for a controlled and targeted increase of temperature. This heating can potentially amplify electroporation effects by increasing energy and thus the rate of molecular movement. Furthermore, although temperature increase is often taken in to account as an undesirable effect in medical applications of electroporation [27], it is well recognized and utilized for its synergistic benefits in fields such as food processing [28,29]. In addition to the energy increase resulting from the temperature rise, the high-frequency wave itself could improve molecular

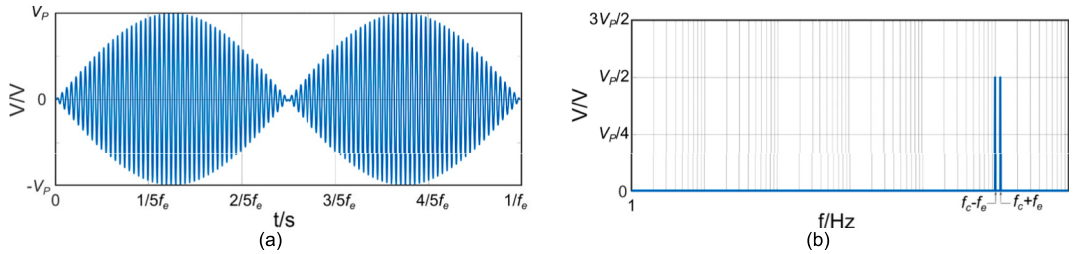

Fig. 5. Amplitude modulation waveform: (a) temporal waveform, and (b) harmonic content.

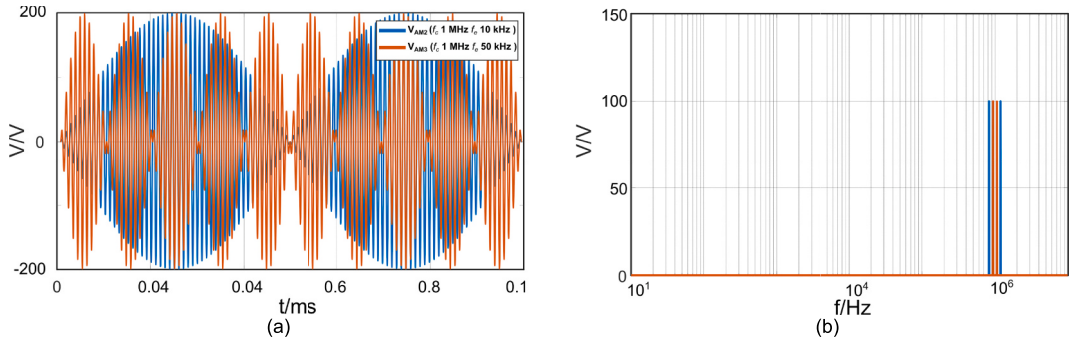

Fig. 6. Three representative protocols of amplitude modulation: (a) temporal waveform, and (b) harmonic content.

mobility due to the enhanced energy transfer and the high-frequency electromagnetic field variations produced with high-frequency waves, making this strategy potentially valuable in electroporation applications such as gene electrotransfer [30].

Sequential application waveform v_{CA}(t), as shown in Fig. 7, consisted of the sequential application of two sine functions during the time t_{ph} and t_d with amplitudes of V_H and V_L, and frequencies of f_L and f_H, respectively:

$$v_{CA}(t) = \begin{cases} V_H sin(2\pi f_H t) & 0 < t \le t_{ph} \\ V_L sin(2\pi f_L t) & (t_{ph} + t_d) < t \le (t_{ph} + t_d + t_e) \\ 0 & t < 0 | t_{ph} < t \le t_d | t < (t_{ph} + t_d + t_e) \end{cases} \quad (4)$$

The aim of this combination of waveforms was to sequentially apply both harmonics, rather than combining them, with the goal of using the high frequency to induce a controlled temperature increase and the low frequency to generate electroporation. This approach presented several differences from the previous strategies. First, a high-frequency waveform of extended duration t_{ph}, lasting tens of seconds and with a very low amplitude V_H, was tested. The goal was to achieve a controllable temperature increase with a moderate peak temperature T_{Max}, while avoiding occurrence of electroporation. Next, three target temperatures T_T were selected, and a purely sinusoidal low-frequency treatment was evaluated. The amplitude V_L was chosen to be sufficient to induce a low level of electroporation. Finaly, as it is shown in Fig. 7, with continuous temperature monitoring, the low-frequency harmonic waveform is applied once the target temperature T_T is reached, following a waiting period t_d.

As illustrated in Fig. 7, a 1 MHz sine wave with an amplitude V_H of less than 10 V was applied for the first 60 s of heating time tph, allowing the temperature to rise in a controlled and monitorized way to 42 °C of T_{Max}. To assess the impact of temperature, three target temperatures T_T were initially selected: 35 °C, 32 °C, and 28 °C, with the latter matching the sample's initial temperature. Once the sample temperature reached 42 °C, the sample was allowed to cool down during t_d up to achieve the target temperature T_T, at which point a single 5 ms burst of a 10 kHz sine wave with a V_L of 85 V was applied.

For the CHO cell line, the protocols used are detailed in Table 7 and Table 8 and are the ones that were initially proposed. However, the protocols for the H9c2 line are presented in Table 9 and Table 10 and unlike in the previous line it was necessary to add 2 more protocols and adjust V_L. The V_{H2} and V_{SA4} protocols were included to achieve a greater temperature increase and V_L was reduced to achieve a more controlled temperature increase. As the results indicate, the H9c2 line appears less sensitive within the initially selected target range.

Fig. 8 shows the measurements performed in 3 application examples, one for each target temperature case.

Table 7
Purely Sinusoidal Protocols in CHO.

	V_P /V	V_{RMS} (V)	f (kHz)	t_{ph}- t_e (ms)	ΔT(°C)
V_H	9	6.4	1000	60,000	14
V_L	85	60.1	10	5	1.25

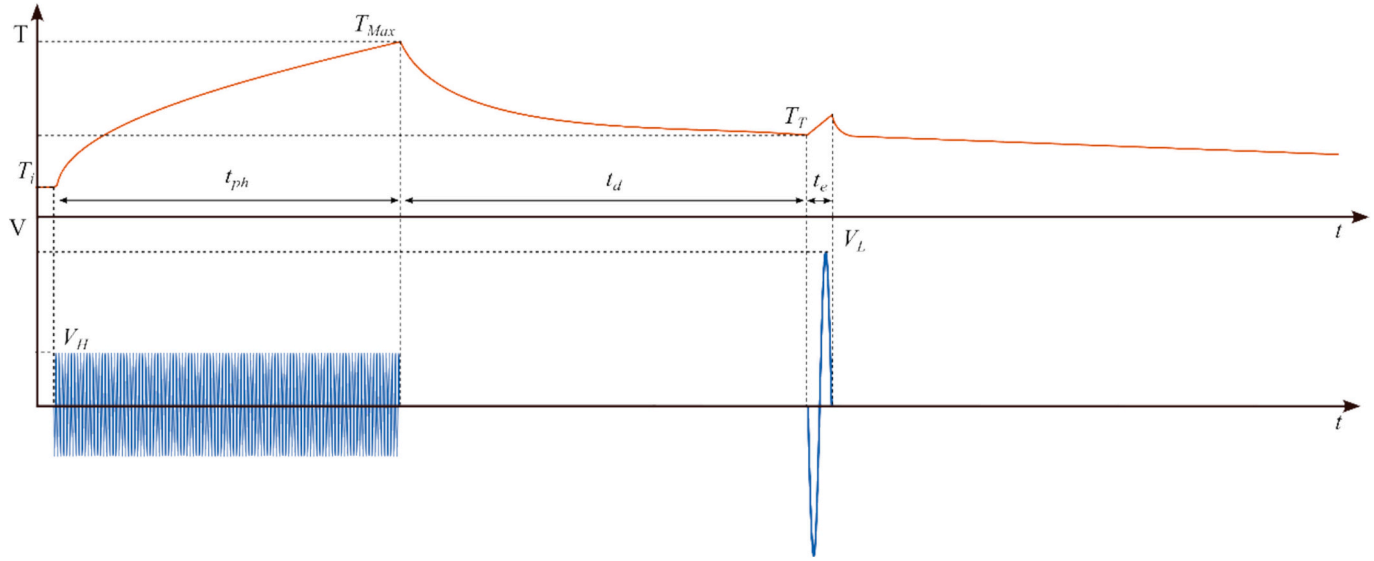

Fig. 7. Representation of the thermal evolution and the applied voltage in the sequential application.

Table 8
Sequential Application Protocols in CHO.

	T_i (°C)	T_{Max} (°C)	T_T (°C)	t_d (s)
V_{SA1}	28	42	35	50
V_{SA2}	28	42	32	110
V_{SA3}	28	42	28	425

Table 9
Purely Sinusoidal Protocols in H9c2.

	V_P (V)	V_{RMS} (V)	f (kHz)	t_{ph}- t_e (ms)	ΔT(°C)
V_{H1}	8	5.7	1000	60,000	14
V_{H2}	8	5.7	1000	150,000	27
V_L	85	60.1	10	5	1.25

Table 10
Sequential Application Protocols in H9c2.

	T_i (°C)	T_{Max} (°C)	T_T (°C)	t_d (s)
V_{SA1}	28	42	35	50
V_{SA2}	28	42	32	110
V_{SA3}	28	42	28	425
V_{SA4}	28	42	40	50

2.5. Analysis

2.5.1. Flow cytometer

Before treatment 6 µl of propidium iodide (PI) (final concentration of PI was 100 mg/µl) was added to 60 µl of cell suspension with density of 1×10^6 cells/ml. Afterwards 60 µl of dyed cell suspension was transferred to 1 mm aluminum cuvettes (VWR International, USA) prior to pulse treatment. Three minutes after treatment, the sample was removed from the cuvette and the uptake of PI in cells was analyzed by the flow cytometer (Attune NxT; Life Technologies, Carlsbad, CA, USA) using 488 nm blue laser and 574/26 nm band-pass filter. An analysis of 10.000 events was performed by Attune Nxt software. Using dot plots, debris and clusters were excluded from our samples and only single cells were taken into analysis. Fluorescence intensity histograms were used to determine the percentage of PI permeabilized cells. Gating was set according to sham control (no treatment).

2.5.2. Survival test

In viability assay 60 µl of cell suspension with density of 1×10^6 cells/ml was transferred to 1 mm aluminum cuvettes (VWR International, USA). After the treatment cells were diluted in fresh growth media. Then 100 µl of treated cell suspension (1.5×10^4 CHO cells, 1×10^4 H9c2 cells) was transferred to 96-well plate (TPP, Switzerland) and incubated at 37 °C and humidified 5 % CO_2 atmosphere for 24 h. According to manufacturer's instructions (CellTiter 96 AQueous One Solution Cell Proliferation Assay, Promega, USA) 20 µl of MTS tetrazolium compound was added to the samples and returned to the incubator. After 2 h the absorbance of formazan (reduced MTS tetrazolium compound) was measured with a spectrofluorometer (Tecan Infinite M200, Tecan, Austria) at 490 nm. Percentage of viable cells was obtained by the normalization of sample absorbance to the absorbance of the sham control (no treatment).

3. Results

The proposed proof of concept was evaluated for three harmonic combination strategies using an *in vitro* model and a common setup. To enable useful comparisons across different experiments and strategies, treatment protocols were aligned as closely as possible. Temporal parameters for all treatments were standardized to 20 bursts of 5 ms each, applied at a frequency of 1 Hz. To maximize the sensitivity range of the biological tests and fully utilize the setup's features, the data presented in Fig. 9 were collected during initial characterization. The initial protocol V_{IP}, comprising a pure sine wave with an amplitude of 106 V and predefined time parameters, was used for both amplitude (Fig. 9 (a)) and frequency (Fig. 9 (b)) characterization. This protocol was evaluated to confirm its minimal impact while enabling variations in amplitude and frequency. By leveraging the approach that utilizes the generator's features, it becomes possible to apply protocols that generate a response in the permeability assay across the full sensitivity range, from 0 to 100 %, thereby enabling the study of the phenomenon throughout its entire range.

The highest frequency used across all experiments was 1 MHz. As shown in Fig. 9 (a), application of a pure sine wave at this frequency leads to complete cell response, as over 99 % of CHO and H9c2 cells can be permeabilized with the proposed setup. Additionally, application of sinusoidal treatments with a fixed amplitude V_P of 106 V and varying

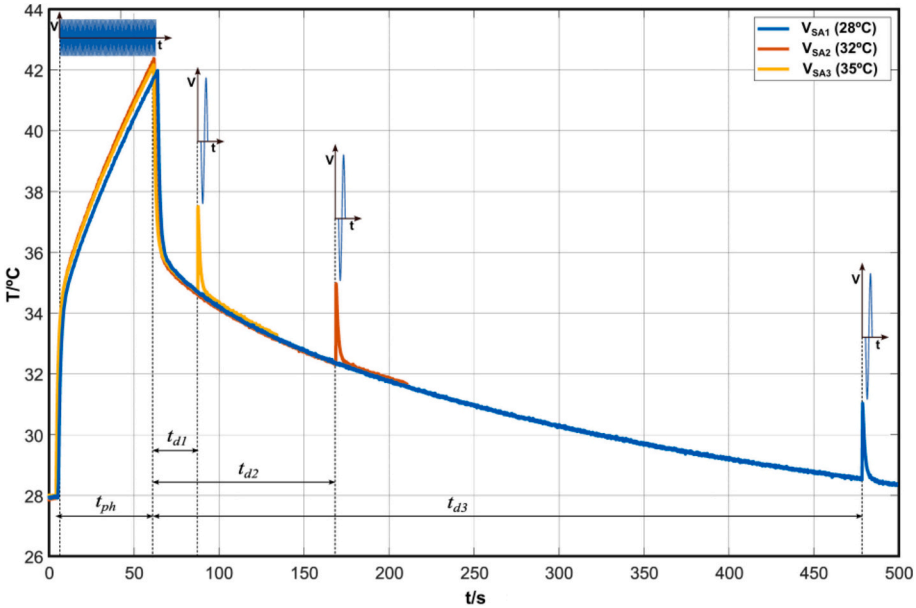

Fig. 8. Thermal measurements recorded in three representative protocols: V_{SA3} with T_T of 28 °C (blue), V_{SA2} with T_T 32 °C (red), and V_{SA1} with T_T 35 °C (yellow). (For interpretation of the references to colour in this figure legend, the reader is referred to the web version of this article.)

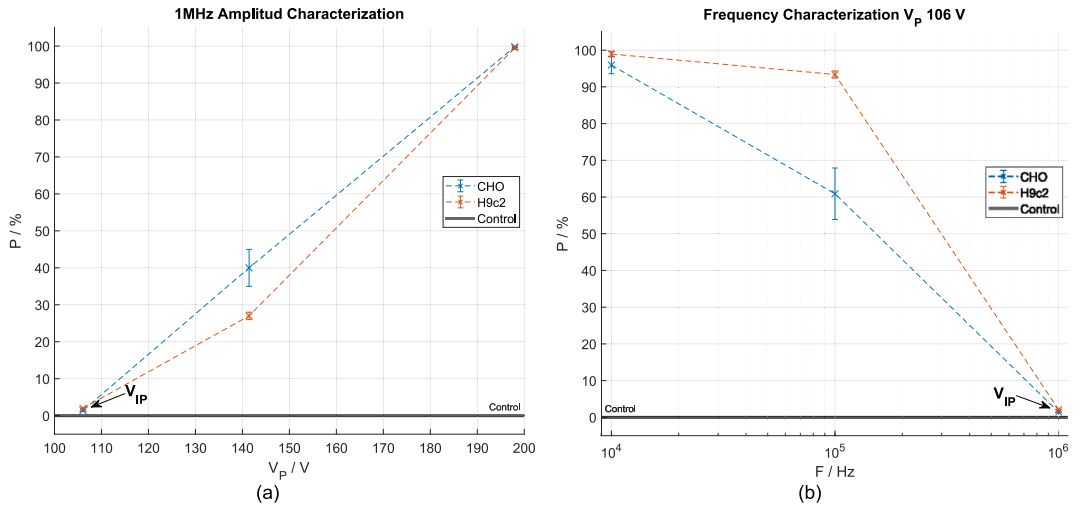

Fig. 9. Permeability curves for H9c2 (red) and CHO (blue) cell lines using a sinusoidal waveform: (a) Amplitude response at 1 MHz and (b) frequency response at a constant amplitude of 106 V. (For interpretation of the references to colour in this figure legend, the reader is referred to the web version of this article.)

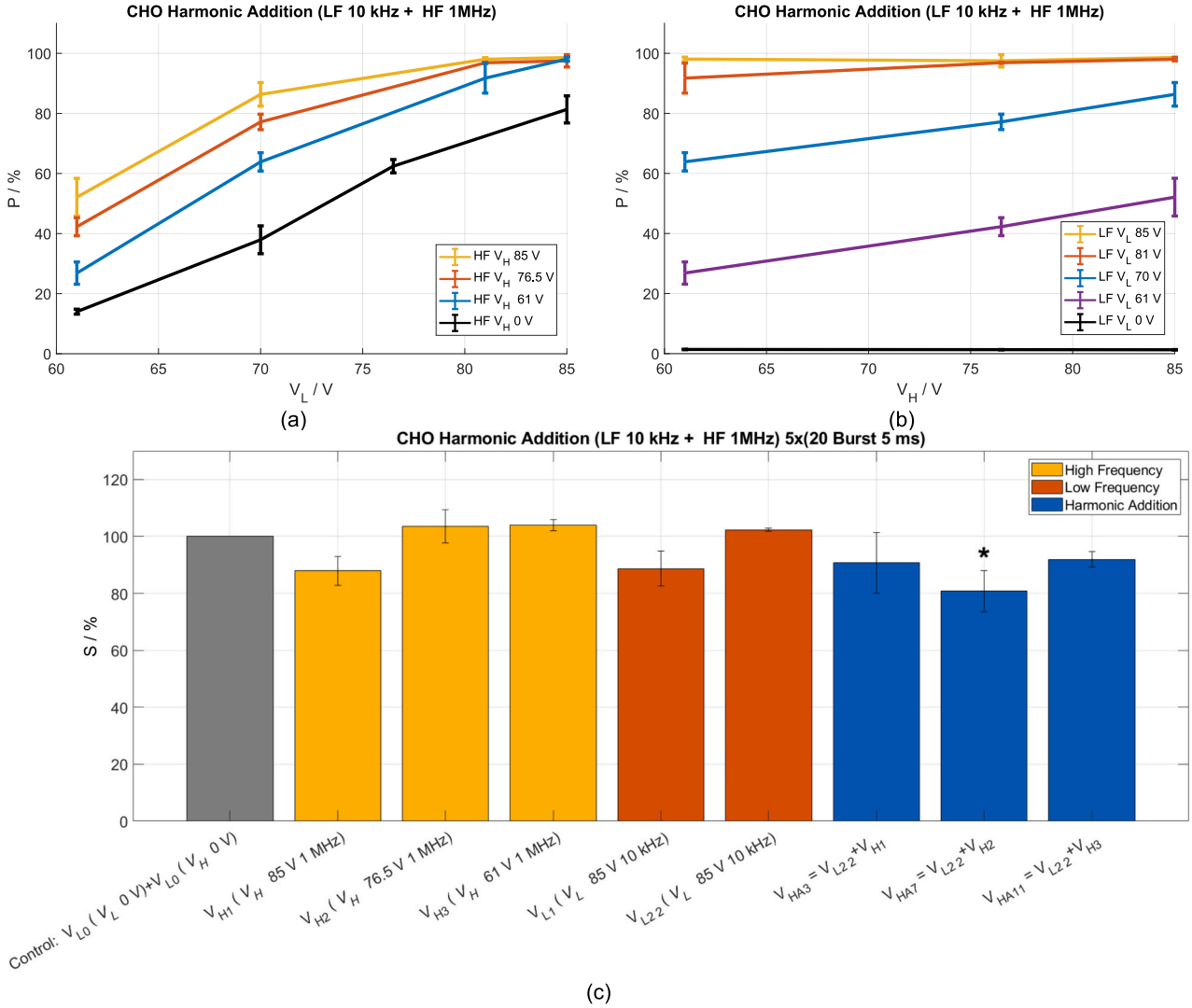

Fig. 10. Results of CHO cell line using a harmonic addition waveform: (a) Permeability curves organized by low-frequency harmonic amplitude V_L, with high-frequency harmonic amplitude curves V_H parameter at 85 V (yellow), 76.5 V (red), 61 V (blue), and 0 V (black), and (b) permeability curves organized by high-frequency harmonic amplitude V_H, showing low-frequency harmonic amplitude curves V_L parameter at 85 V (yellow), 81 V (red), 70 V (blue), 61 V (purple), and 0 V (black). Survival results applied 5 repetitions (c): Yellow indicates results from the high-frequency pure sinusoidal waveform, red represents results from the low-frequency pure sinusoidal waveform, and blue shows results from the harmonic addition.* marks electroporated samples in which survival results are statistically significantly different compared to the control. (For interpretation of the references to colour in this figure legend, the reader is referred to the web version of this article.)

frequency from 10 kHz to 1 MHz showed that cell permeabilization in CHO and H9c2 cells was frequency-dependent (Fig. 9 (b)). In both cases H9c2 cells resulted in similar permeabilization efficacy as in CHO cell line. However, the frequency-dependent permeability response in H9c2 line revealed a somewhat different response from that observed in the CHO cell line.

Fig. 10 presents the results from the experiment evaluating the harmonic addition strategy in CHO line. In this experiment, using 20 bursts of 5 ms, 4 V_L for the 10 kHz harmonic and 3 V_H for the 1 MHz harmonic were selected. These harmonics were evaluated independently and then combined, resulting in a total of 7 purely sinusoidal treatments V_H an V_L (Table 1) and 12 combined treatments V_{HA} (Table 2). Fig. 10 (a) shows the increased cell permeability across all treatments as the harmonic content of the 10 kHz waveform increased, irrespective of the 1 MHz harmonic content. This same permeability increase could be observed in function of 1 MHz waveform in Fig. 10 (b), though with a smoother slope. It was also clear that treatments with distinct harmonic compositions could achieve equivalent permeability levels. For example, a purely sinusoidal 10 kHz treatment V_{L1} with V_L 85 V yielded a similar permeability increase to a combined treatment V_{HA2}, combination of treatments V_{H1} (85 V at 1 MHz) and V_{L2_1} (70 V at 10 kHz).

Treatments with comparable permeability results were then evaluated for cell viability. To make the effects measurable, each treatment was repeated five times, resulting in a total of 100 bursts of 5 ms. It was not possible to increase this treatment length due to overheating of the sample and observed increase in electrochemical reactions. Fig. 10 (c) shows the results of the high frequency, low frequency and combined treatments with equivalent permeability effects (sinusoidal 10 kHz treatment V_{L1} with V_L 85 V yielded a similar permeability increase to a combined treatment V_{HA3}, combination of treatments V_{H1} (85 V at 1 MHz) and V_{L2_1} (70 V at 10 kHz).

Fig. 11 presents the results in H9c2 line. In this experiment, 20 bursts of 5 ms, 3 V_L for the 10 kHz harmonic and 3 V_H for the 1 MHz harmonic were used. These harmonics were evaluated independently and then combined, resulting in a total of 7 purely sinusoidal treatments V_H an VL

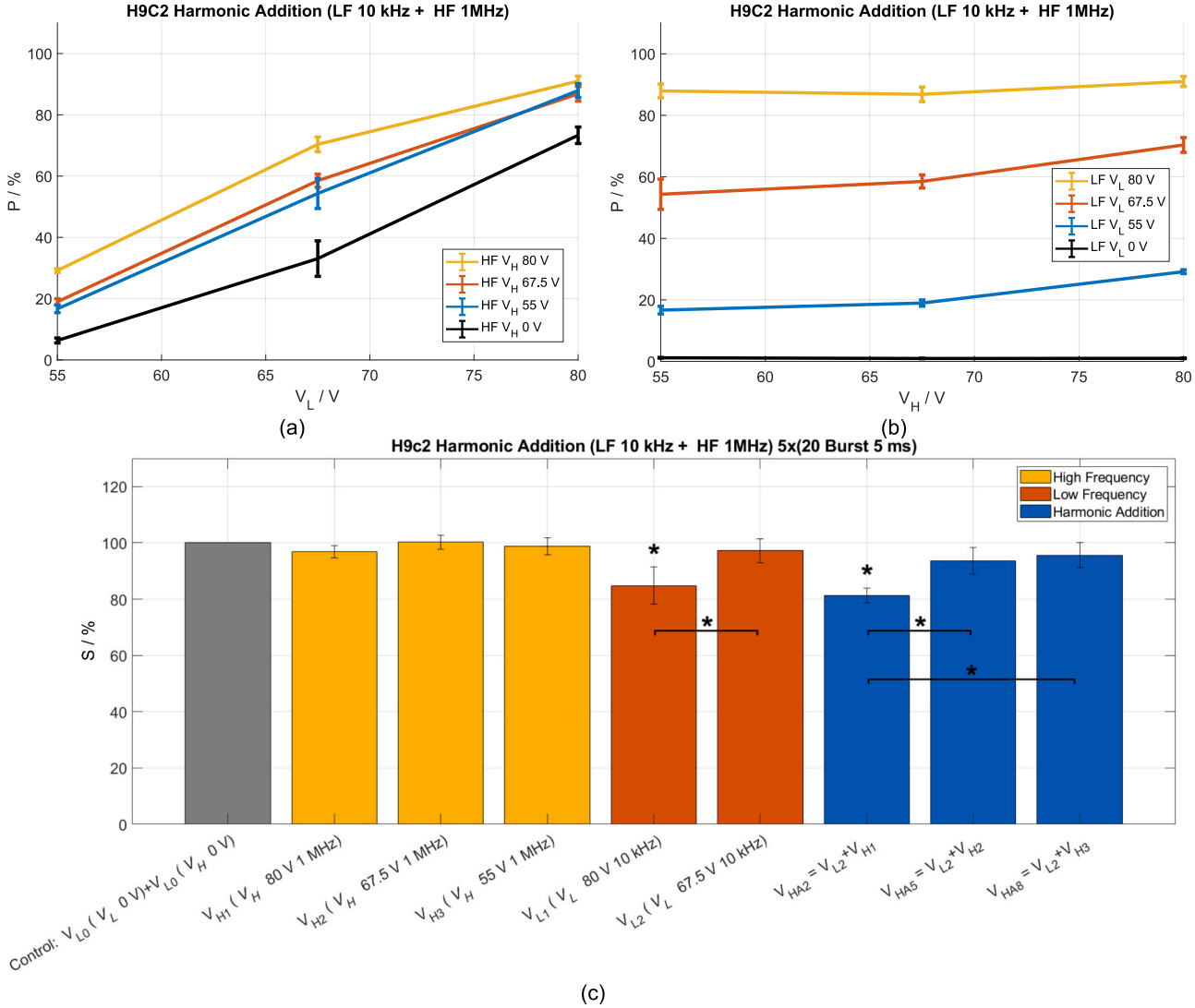

Fig. 11. Results of H9c2 cell line using a harmonic addition waveform: (a) Permeability curves showing dependance on low-frequency harmonic amplitude V_L, with high-frequency harmonic amplitude curves V_H parameter at 80 V (yellow), 67.5 V (red), 55 V (blue), and 0 V (black), and (b) permeability curves organized by high-frequency harmonic amplitude V_H, showing low-frequency harmonic amplitude curves V_L parameter at 80 V (yellow), 67.5 V (red), 55 V (blue), and 0 V (black). Survival results applied 5 repetitions (c): Yellow indicates results from the high-frequency pure sinusoidal waveform, red represents results from the low-frequency pure sinusoidal waveform, and blue shows results from the harmonic addition. * marks electroporated samples in which survival results are is statistically significantly different compared to the control or between the groups marked. (For interpretation of the references to colour in this figure legend, the reader is referred to the web version of this article.)

(Table 3) and 12 combined treatments V_{HA} (Table 4). Fig. 11 (a) shows the increase in cell permeability across all treatments as the harmonic content of the 10 kHz waveform increases, irrespective of the 1 MHz harmonic content. This same permeability increase could be observed in function of 1 MHz waveform in Fig. 11 (b), though with a smoother slope. Although the slopes were not the same, the trend in H9c2 cell line is the same as in the CHO, and equivalent treatments could be found such as a purely sinusoidal 10 kHz treatment V_{L1} with V_L 80 V yielded a similar permeability increase to a combined treatment V_{HA2}, combination of treatments V_{H1} (80 V at 1 MHz) and V_{L2} (67.5 V at 10 kHz).

Treatments with comparable permeability results were then evaluated for cell viability. To make the effects measurable, each treatment was repeated five times, resulting in a total of 100 bursts of 5 ms. It was not possible to increase this treatment length due to overheating of the sample and observed increase in electrochemical reactions. Fig. 11 (c) shows the results of the high frequency, low frequency and combined treatments with equivalent permeability effects (sinusoidal 10 kHz treatment V_{L1} with V_L 80 V yielded a similar permeability increase to a combined treatment V_{HA2}, combination of treatments V_{H1} (80 V at 1 MHz) and V_{L2} (67.5 V at 10 kHz). Although the results were not fully conclusive, it was appreciably clearer in this cell line that pure high-frequency treatments had a reduced impact on cell viability compared to pure low-frequency treatments.

Fig. 12 presents the results from the experiment evaluating the amplitude modulation.

strategy. First, Fig. 12 (a) shows the results of the amplitude modulation with a f_c of 1 MHz, a V_P of 200 V, and an V_{RMS} of 100 V. These results were compared in the same figure as those obtained from two sinusoidal treatments (dashed lines) at 1 MHz, first with a V_P of 200 V and second with a V_{RMS} of 100 V. Fig. 12 (b) shows the results of the modulation with a f_c of 500 kHz, a V_P of 150 V, and a V_{RMS} of 75 V. These results were compared in the same figure with those obtained from two sinusoidal treatments (dashed lines) at 500 kHz, each with a V_P of 150 V and a V_{RMS} of 75 V, respectively. For both f_c, the amplitude modulated treatments showed a stronger effect than a pure sine wave with the same V_{RMS}, though they remained less effective than a sine wave with the same V_P. Additionally, unlike the behavior observed in Fig. 9 (b), the frequency of the envelope did not impact the outcome, as reductions only occurred when the envelope and carrier frequencies were in close proximity.

Fig. 12 (b) shows the results of V_{AM} protocols with a f_c of 1 MHz a V_P of 200 V, and a V_{RMS} of 100 V. These results are compared in the same figure as those obtained from two purely sinusoidal treatments (dashed lines) at 1 MHz, one with a V_P of 200 V and the second with V_{RMS} of 100 V. Fig. 12 (c) shows the results of the modulation with a f_c of 500 kHz, a V_P of 150 V, and a V_{RMS} of 75 V. These results were compared in the same figure with those obtained from two purely sinusoidal treatments (dashed lines) at 500 kHz, each with a V_P of 150 V and a V_{RMS} of 75 V,

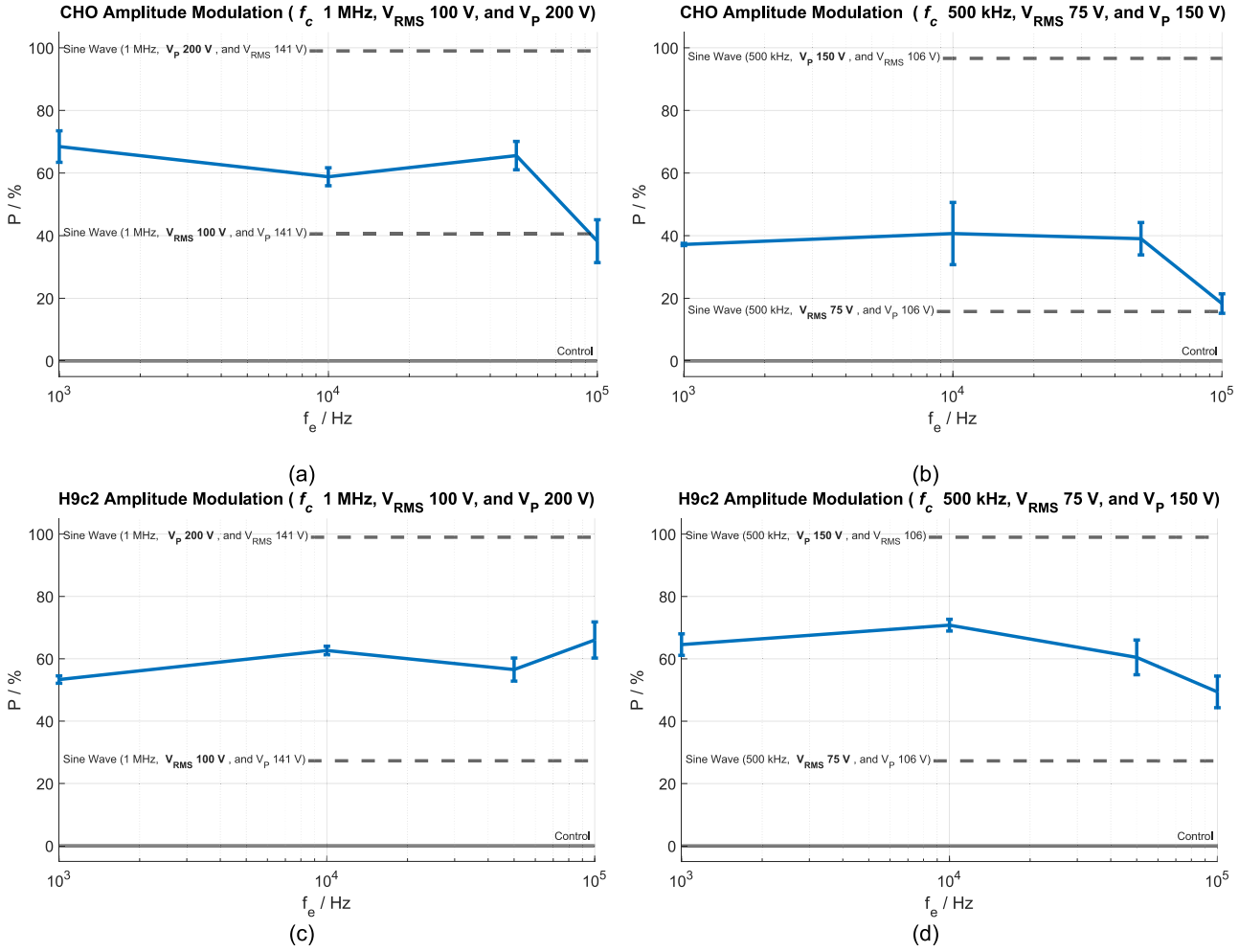

Fig. 12. Permeability results using a harmonic amplitude modulation waveform: (a) for CHO and (c) for H9c2, in blue, the permeability curve as a function of the envelope frequency f_e with a carrier frequency f_c of 1 MHz, and in dashed gray, the mean values of pure sine waves with the same f_c and equal V_P and V_{RMS} values as the amplitude modulation protocols. (b) for CHO and (d) for H9c2, in blue, the permeability curve as a function of the envelope frequency f_e with a carrier frequency f_c of 500 KHz, and in dashed gray, the mean values of pure sine waves with the same f_c and equal V_P and V_{RMS} values as the amplitude modulation protocols. (For interpretation of the references to colour in this figure legend, the reader is referred to the web version of this article.)

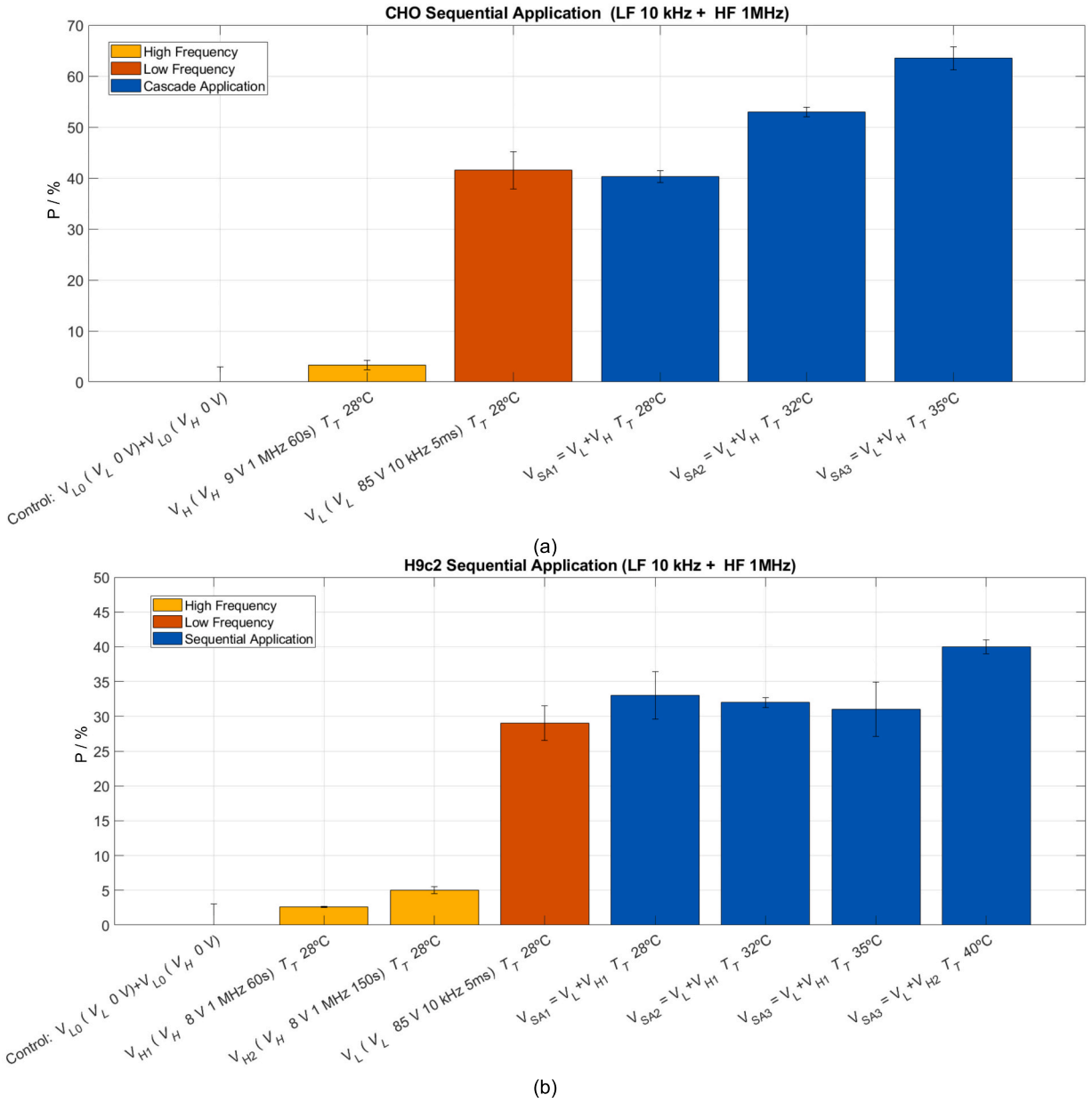

Fig. 13. Permeability results using sequential application: (a) for the CHO cell line: Yellow indicates results from the high-frequency pure sinusoidal waveform, red represents results from the low-frequency pure sinusoidal waveform, and blue shows results from the sequential application. (b) for H9c2 cell line: Yellow indicates results from the high-frequency pure sinusoidal waveform, red represents results from the low-frequency pure sinusoidal waveform, and blue shows results from the sequential application. (For interpretation of the references to colour in this figure legend, the reader is referred to the web version of this article.)

respectively. Similar as in CHO line, for both frequencies, the amplitude modulated treatments showed a stronger effect than a pure sine wave with the same V_{RMS} 75 V, though they remained less effective than a sine wave with the same V_P 150 V. Also, unlike the behavior observed in Fig. 9 (b), the frequency of the envelope did not impact the outcome, as reductions only occurred when the envelope and carrier frequencies were in proximity.

Fig. 13 presents the results from 3rd strategy – sequential application of the harmonics. Fig. 13 (a) presents the results from the permeability test on the CHO cell line. The data show that preheating at high frequency has minimal impact at an initial temperature of 28 °C, as the effects are constant with or without preheating. However, when the initial sample temperatures are raised to 32 °C and 35 °C, a distinct improvement in treatment effectiveness becomes apparent.

The results for the H9c2 cell line differ from those obtained with the CHO cell line. As shown in Fig. 13 (b), the initial temperatures that enhanced permeabilization in the CHO line had no effect on the H9c2 cells. To achieve increased permeability in this model, a secondary heating protocol of longer duration (150 s) with a peak temperature of 55 °C was necessary to reach a target temperature of 40 °C for low frequency application. The results indicate that this extended heating protocol alone had only a minor effect on permeabilization, but it significantly amplified the impact of the low-frequency harmonic.

Survival assays were also performed; however, they did not show any difference in survival (data not shown).

4. Discussion

This paper presents an evaluation of combining high and low-frequency harmonics in electroporation. A new power electronics system was developed to allow carrying out this study, enabling the assessment of three different strategies *in vitro*: harmonic addition,

amplitude modulation an sequential application. A characterization of the effect of sine waves in an *in vitro* model has been carried out, building on previous works [3,6].

The experiments performed using the harmonic addition strategy within the studied range shows that combining two harmonics of different frequencies produces a greater effect than applying each harmonic separately. The impact of the resulting wave is mainly governed by the low-frequency harmonic. *I.e.*, increasing the amplitude of the low-frequency harmonic significantly enhances the effect of the combined wave, while increasing the amplitude of the high-frequency harmonic has a comparatively smaller impact. These findings align with observations from the frequency characterization, suggesting that the permeability effects of both harmonics are additive. When effects were compared in terms of V_{RMS}, pure low-frequency harmonics demonstrated greater efficiency than harmonic addition waveforms, and no clear synergy was observed from combining high- and low-frequency harmonics. However, experimental observations also revealed that harmonic addition protocols and pure low-frequency harmonic protocols can achieve similar results in terms of permeability. Therefore, a harmonic addition protocol equivalent to a low-frequency harmonic in terms of permeability could potentially enhance mobility of molecules at the membrane level or help to reduce electrochemical reactions at the electrode -electrolyte surface interface.

The evaluation of amplitude modulated waveforms yielded new insights. Within the studied frequency range and using an *in vitro* model, amplitude modulated waves produced a stronger effect than a pure high-frequency sine wave with the same V_{RMS}. However, amplitude-modulated waveforms were less effective than a pure sine wave with the same V_P. Additionally, the envelope frequency showed no clear impact on treatment efficacy, except for a decrease in effectiveness when the frequency of the envelope approaches the carrier frequency. This suggests that the increased effect, when comparing waves by V_{RMS}, likely resulted from the higher peak amplitude of the amplitude modulated wave at equivalent V_{RMS} levels. If this effect were due to membrane non-linear behavior [31], a distinct increase would be expected as the envelope frequency decreases, similar to the frequency response seen in pure sinusoidal waves. Therefore, these non-linear effects at the membrane level are not observed in the model used or within the studied frequency range, and it is currently unlikely that they can be technologically achieved. Additionally, considering the results of harmonic addition, waveform shape modification had no significant effect unless the waveform contained low-frequency harmonic content. Furthermore, unlike in harmonic addition strategy, the electrochemical reactions and molecular diffusion effects induced by amplitude-modulated waves were likely very similar to those produced by a pure high-frequency sine wave, offering no clear advantages for using amplitude modulation waveforms.

Regarding temperature, a combination of temperature and electroporation treatment has been shown to increase electroporation before [28,29]. Sequential applications have been shown to be an effective method for achieving controlled heating. However, while this approach had enhanced the electroporation effect in both models, the outcome varied between cell lines used. In H9c2 cell line, for example, the required temperature increase could lead to undesired thermal effects. Although this proof of concept primarily assesses the strategy's feasibility, the potential of control it offers is compelling. Continuous temperature regulation through high-frequency harmonics could enable real-time, small-signal impedance monitoring [32], allowing for more precise treatment control.

After evaluating the three proposed strategies that combine high and low frequencies, sequential application and harmonic addition emerge as the most promising options. While their potential to enhance treatment efficiency, facilitate molecular diffusion, and reduce electrochemical reactions is highlighted, these aspects remain to be demonstrated. Therefore, these aspects should be considered as potential goals for future research, where total energy could serve as a valuable parameter for assessing treatment efficiency. While V_{RMS} is the chosen variable for comparing the three proposed strategies in this proof of concept, for an in-depth study of a single strategy, a precise calculation of the total energy would also be valuable to compare the efficiency of the treatments.

5. Conclusions

A proof of concept was presented to assess the feasibility of three different strategies for combining high- and low-frequency harmonics in electroporation protocols. The study required the development of specialized power electronics hardware and extensive experimentation to evaluate each strategy. The results indicate promising potential for the use of high- and low-frequency harmonic combinations in electroporation, with the most effective approaches identified as harmonic combination and sequential application of HF followed by LF.

Further research in this area requires the development of technology capable of generating high-frequency arbitrary waveforms, exceeding the MHz range, with high output voltage and current levels, reaching kilovolts and tens of amperes. Therefore, developing versatile high-frequency biomedical platforms could be highly beneficial in electroporation applications.

Funding

This work was partly supported by Projects, PID2022–136621OB-I00, PDC2023–145837-I00, and PI21/00440 co-funded by MICIU/AEI/10.13039/501100011033, by Instituto de Salud Carlos III (ISCIII), by "ERDF A way of making Europe", by the "European Union NextGenerationEU/PRTR", by the DGA-FSE, and by the DGA-FSE, and by Margarita Salas fellowship by the MIU and NextGenerationEU, convocatoria de ayudas para la recualificación del sistema universitario español para 2021–2023. The study was supported to by the Slovenian Research Agency (ARIS) within research programs no. J2–50068 and P2–0249. The work has been performed within the laboratories of the Infrastructural Center of the University of Ljubljana, which is financially supported by the Slovenian Research Agency through infrastructural grant I0–0022.

Credit authorship contribution statement

Borja López-Alonso: Writing – review & editing, Writing – original draft, Visualization, Validation, Supervision, Software, Resources, Project administration, Methodology, Investigation, Formal analysis, Data curation, Conceptualization. **Tamara Polajžer:** Writing – review & editing, Visualization, Validation, Supervision, Methodology, Investigation, Formal analysis, Data curation, Conceptualization. **Matej Reberšek:** Writing – review & editing, Supervision, Methodology, Conceptualization. **Héctor Sarnago:** Writing – review & editing, Supervision, Software, Methodology, Investigation, Formal analysis, Conceptualization. **Óscar Lucía:** Writing – review & editing, Project administration, Methodology, Funding acquisition, Conceptualization. **Damijan Miklavčič:** Writing – review & editing, Project administration, Methodology, Funding acquisition, Data curation, Conceptualization.

Declaration of competing interest

The authors declare that they have no known competing financial interests or personal relationships that could have appeared to influence the work reported in this paper.

Data availability

Data will be made available on request.

References

[1] S.Y. Ho, G.S. Mittal, Electroporation of cell membranes: a review, Crit. Rev. Biotechnol. 16 (4) (1996) 349–362.

[2] T. Kotnik, L. Rems, M. Tarek, D. Miklavcic, Membrane Electroporation and Electropermeabilization: Mechanisms and Models, Annu. Rev. Biophys. *48* (2019) 63–91. K. A. Dill, Ed. (Annual Review of Biophysics.

[3] T. Kotnik, G. Pucihar, M. Reberšek, D. Miklavčič, L.M. Mir, Role of pulse shape in cell membrane electropermeabilization, Biochimica et Biophysica Acta (BBA) - Biomembranes 1614 (2) (2003) 193–200.

[4] C. Merla, A.G. Pakhomov, I. Semenov, P.T. Vernier, Frequency spectrum of induced transmembrane potential and permeabilization efficacy of bipolar electric pulses, BBA-Biomembranes 1859 (7) (2017) 1282–1290.

[5] O. Lucia, H. Sarnago, T. Garcia-Sanchez, L.M. Mir, J.M. Burdio, Industrial electronics for biomedicine: a new Cancer treatment using electroporation, IEEE Ind. Electron. Mag. 13 (4) (2019) 6–18.

[6] T. Garcia-Sanchez, et al., Successful tumor Electrochemotherapy using sine waves, IEEE Trans. Biomed. Eng. 67 (4) (2020) 1040–1049.

[7] C.B. Arena, et al., High-frequency irreversible electroporation (H-FIRE) for non-thermal ablation without muscle contraction, Biomed. Eng. Online 10 (2011). Art. (no. 102).

[8] M.L. Yarmush, A. Golberg, G. Sersa, T. Kotnik, D. Miklavcic, Electroporation-Based Technologies for Medicine: Principles, Applications, and Challenges, in: M. L. Yarmush (Ed.), Annual Review of Biomedical Engineering 16, 2014, pp. 295–320. Annual Review of Biomedical Engineering.

[9] A. Vizintin, S. Markovic, J. Scancar, D. Miklavcic, Electroporation with nanosecond pulses and bleomycin or cisplatin results in efficient cell kill and low metal release from electrodes, Bioelectrochemistry 140 (2021). Art. (no. 107798).

[10] L. Retelj, G. Pucihar, D. Miklavcic, Electroporation of intracellular liposomes using nanosecond electric pulses-a theoretical study, IEEE Trans. Biomed. Eng. 60 (9) (2013) 2624–2635.

[11] C.G. Yao, et al., Bipolar microsecond pulses and insulated needle electrodes for reducing muscle contractions during irreversible electroporation, IEEE Trans. Biomed. Eng. 64 (12) (2017) 2924–2937.

[12] R. Fusco, E. Di Bernardo, V. D'Alessio, S. Salati, M. Cadossi, Reduction of muscle contraction and pain in electroporation-based treatments: an overview, World J. Clinical Oncol. 12 (5) (2021) 367–381.

[13] A. Cvetkoska, A. Macek-Lebar, P. Trdina, D. Miklavcic, M. Rebersek, Muscle contractions and pain sensation accompanying high-frequency electroporation pulses, Sci. Rep. 12 (1) (2022). Art. (no. 8019).

[14] B. López-Alonso, P. Briz, H. Sarnago, J.M. Burdio, Optimizing IRE targeting using multi-electrode structure and biomedical multi-output generator, COMPEL - The Int. J. Comput. Math. Electric. electron. Eng. 43 (2024) 1184–1196.

[15] B. Lopez-Alonso, H. Sarnago, J.M. Burdio, P. Briz, O. Lucia, Multi-Electrode Architecture Modeling and Optimization for Homogeneous Electroporation of Large Volumes of Tissue, Energies 14 (7) (2021). Art. (no. 1892).

[16] B. López-Alonso, H.L.Ó. Sarnago, J.M. Burdío, Multiple-Output Generator for Omnidirectional Electroporation and Real-Time Process Monitoring, 2021 IEEE Appl. Power Electron. Conf. Exposition (APEC) (2021) 1388–1392.

[17] R. Sundararajan, Nanosecond electroporation: another look, Mol. Biotechnol. 41 (1) (2009) 69–82.

[18] J. Dermol, D. Miklavcic, Predicting electroporation of cells in an inhomogeneous electric field based on mathematical modeling and experimental CHO-cell permeabilization to propidium iodide determination, Bioelectrochemistry 100 (2014) 52–61.

[19] E. Goldberg, C. Suárez, M. Alfonso, J. Marchese, A. Soba, G. Marshall, Cell membrane electroporation modeling: a multiphysics approach, Bioelectrochemistry 124 (2018) 28–39.

[20] U. Cegovnik, S. Novakovic, Setting optimal parameters for in vitro electrotransfection of B16F1, SA1, LPB, SCK, L929 and CHO cells using predefined exponentially decaying electric pulses, Bioelectrochemistry 62 (1) (2004) 73–82.

[21] K. Asadipour, M.B. Hani, L. Potter, B.L. Ruedlinger, N.C.L. Lai, S.J. Beebe, Nanosecond pulsed electric fields (nsPEFs) modulate Electron transport in the plasma membrane and the mitochondria, Bioelectrochemistry 155 (2024). Art. (no. 108568).

[22] Y.C. Liu, W.Y. Lin, Y.R. Jhang, S.H. Huang, C.P. Wu, H.T. Wu, Efficiency of DNA transfection of rat heart myoblast cells H9c2(2-1) by either Polyethyleneimine or electroporation, Appl. Biochem. Biotechnol. 164 (7) (2011) 1172–1182.

[23] I. Kaminska, et al., "electroporation-induced changes in normal immature rat myoblasts (H9C2)," (in eng), Gen. Physiol. Biophys. 31 (1) (2012) 19–25.

[24] H. Sarnago, J.M. Burdío, T. García-Sánchez, L.M. Mir, I. Alvarez-Gariburo, O. Lucía, GaN-based versatile waveform generator for biomedical applications of electroporation, IEEE Access 8 (2020) 97196–97203.

[25] J. Kulbacka, A. Choromanska, J. Rossowska, J. Wezgowiec, J. Saczko, M.P. Rols, Cell Membrane Transport Mechanisms: Ion Channels and Electrical Properties of Cell Membranes, in: J. Kulbacka, S. Satkauskas (Eds.), Transport across Natural and Modified Biological Membranes and Its Implications in Physiology and Therapy 227, 2017, pp. 39–58. Advances in Anatomy Embryology and Cell Biology.

[26] S.N. Goldberg, D.E. Dupuy, Image-guided radiofrequency tumor ablation: challenges and opportunities - part I, J. Vasc. Interv. Radiol. 12 (9) (2001) 1021–1032.

[27] A.M. Hogenes, et al., The influence of irreversible electroporation parameters on the size of the ablation zone and thermal effects: a systematic review, Technol. Cancer Res. Treatment 22 (2023). Art. (no. 15330338221125003).

[28] G. Saldaña, I. Álvarez, S. Condón, J. Raso, "microbiological aspects related to the feasibility of PEF technology for food pasteurization," (in eng), Crit. Rev. Food Sci. Nutr. 54 (11) (2014) 1415–1426.

[29] Z. Yan, C. Hao, L. Yin, K. Liu, J. Qiu, Simulation of the influence of temperature on the dynamic process of electroporation based on finite element analysis, IEEE Trans. Plasma Sci. 49 (9) (2021) 2839–2850.

[30] M. Kandušer, M. Pavlin, Chapter two - gene Electrotransfer: From understanding the mechanisms to optimization of parameters in tissues, in: A. Iglič (Ed.), Advances in Planar Lipid Bilayers and Liposomes vol. 15, Academic Press, 2012, pp. 77–104.

[31] N. Nasir, M. Al Ahmad, Cells Electrical Characterization: Dielectric Properties, Mixture, and Modeling Theories 1, 2020, p. 9475490.

[32] B. López-Alonso, H. Sarnago, O. Lucía, P. Briz, J.M. Burdío, Real-Time Impedance Monitoring During Electroporation Processes in Vegetal Tissue Using a High-Performance Generator, Sensors 20 (11) (2020). Art. (no. 3158).